Zonotopic and Gaussian Information Filter for High Integrity Localization

Mohammed Salhi and Joelle Al Hage

***Abstract*—The navigation of intelligent vehicles relies on high integrity localization system capable to bound the estimation errors. This paper introduces a zonotopic and Gaussian Kalman filter in informational form for multi-sensor data fusion and confidence domain computation. By integrating stochastic and set membership uncertainties, the proposed filter ensures accurate localization with a non pessimistic confidence domain, thus addressing the challenges posed by traditional techniques. Taking advantage of the informational form, a fault detection and exclusion step is added to enhance filter robustness. Following a zonotope reduction step, a confidence domain computation, considering both Gaussian and zonotopic uncertainties, is proposed in the context of intelligent vehicles. The accuracy and integrity of the approach are assessed using experimental data, including the fusion of GPS and Galileo pseudoranges with camera measurements after a map matching step. Additionally, a comparative analysis is conducted with the classical Kalman filter.**

I. Introduction

Ensuring accurate localization with high integrity represents a significant challenge for the navigation of intelligent vehicles operating on roads. Typically, the localization process relies on the data fusion of multiple sensors including GNSS (Global Navigation Satellite System), dead-reckoning sensors, cameras and Lidar [1], [2].

The Kalman Filter (KF) is commonly used for merging data from various sensors. This filter is designed to be optimal under the assumptions of linear model and Gaussian noise. For vehicle localization, the process of estimating the state through multi-sensor data fusion is vulnerable to noise originating from sensor measurements and environmental factors, such as multipath interference from GNSS signals. The Gaussian assumption is not always justified and can result in inconsistent state estimation, leading to a loss of integrity.

The set-membership techniques provide a good alternative to Bayesian methods and are particularly well suited for bounding errors without relying on assumptions regarding the noise distributions. The application of set-membership techniques to the localization problem has already been explored in the literature [3], [4]. Despite the interesting quality of the set-membership methods in solving problems in a guaranteed way, they are not well suited for high accuracy tasks and have the drawback of being more pessimistic compared to Bayesian approaches. Additionally, the assumption of fully bounded errors made by these approaches is not always verified.

Combining Bayesian and set-membership techniques has been considered in multiple works [5]–[7]. The resulting filters profit from the advantages of the stochastic representation, which is efficient to deal with random noise, and the set membership representation, which is well adapted to deterministic bounded errors.

In [6] the authors introduce an approach that combines set membership based on ellipsoids with a KF for vehicle localization. The filter incorporates both random and set-membership uncertainties through a weighting parameter. This approach needs the execution of nonlinear optimization algorithm at each step, resulting in high computational cost. In [7], an interval KF enhanced by positive definite upper bound was proposed where the state and observation matrices are represented as interval matrices. The complexity of this method is impacted by the presence of numerous interlocking matrix summations. The Zonotopic and Gaussian Kalman Filter (ZGKF) was proposed in [8] by combining set membership principles based on zonotopes with Gaussian uncertainties. The mathematical properties of zonotopes enable computational efficiency, facilitating a straightforward integration with a classical KF.

In this work, we propose a multi-sensor data fusion approach based on the ZGKF to achieve high integrity localization for intelligent vehicles. Integrity, in this context, denotes the confidence in a navigation solution and is associated with an error bound known as the Protection Level (PL) [9]. The ZGKF is well suited to this problematic since it handles both random and Unknown But Bounded (UBB) errors leading to a consistent and non pessimistic localization solution. Noises from GNSS pseudoranges and camera measurements are then modeled as Gaussian and UBB errors and merged with odometer data. The ZGKF is well adapted to model bias that can appear on sensor measurements.

Mathematically equivalent to the ZGKF, the Zonotopic and Gaussian Information Filter (ZGIF) is proposed and developed in this paper, to take advantage of its update step. Similar to the Information Filter (IF) [10], the informational representation of the ZGKF is well suited for multi-sensor data fusion and fault diagnosis, where the update step is formulated as a straightforward summation of information contributions from each measurement. Although the ZGIF allows modeling UBB, large errors still impact the state estimation and need to be addressed separately. A Fault Detection and Exclusion (FDE) procedure is then added, generating residuals based on the

The authors are with Université de Technologie de Compiègne, CNRS, Heudiasyc, France. This work is funded by the ANR ToICar project (ANR-21-CE33-0012) and is part of SIVALab (joint laboratory Renault/Heudiasyc/UTC/CNRS). Email : mohammed.salhi@hds.utc.fr, joelle.al-hage@hds.utc.fr

Mahalanobis distance between the predicted and updated state estimates. After the FDE step, consistent error bounds must be computed, considering both Gaussian and bounded noises. A new PL method based on both the zonotopic and Gaussian uncertainties is proposed after some modifications regarding the reduction of zonotopes.

This paper is organized as follows: Section II presents the ZGKF principle. Section III presents the proposed ZGIF with FDE architecture. The reduction method used for zonotopes is also presented in this section. Section IV presents the case study and the PL computation. Results on real experiment are discussed in Section V.

II. Multi-sensor data fusion using Zonotope and Gaussian Kalman Filter

A. Zonotopes

Zonotopes are a subset of polytopes that admit convexity and symmetry properties. A zonotope $Z(c, R)$ can be fully described by a center point $c \in \mathbb{R}^n$ and a generator matrix $R \in \mathbb{R}^{n \times m}$ as [11] :

$$Z(c, R) = Z(c, [r_1, ..., r_m]) = \{c + \sum_{i=1}^{m} \beta_i . r_i, -1 \leq \beta_i \leq 1\} \tag{1}$$

where $r_i \in R$ are the generator vectors.

Zonotopes are well suited for set-membership techniques due to their properties that make them efficient for numerical computations.

One notable property is their closure under the Minkowsky sum described by the operator $\oplus$ [8]. For two zonotopes $Z_1(c_1, R_1)$ and $Z_2(c_2, R_2)$, their sum is given by $Z_1(c_1, R_1) \oplus Z_1(c_2, R_2) = Z(c_1 + c_2, [R_1, R_2])$. Additionally, zonotopes are closed under linear transformations: $L \odot Z_1(c_1, R_1) = Z_1(L.c_1, L.R_1)$.

Consider a vector $\mathbf{x} \sim Z(c, R)$, the covariation of $\mathbf{x}$ denoted M is defined as [8]:

$$M = cov(Z(c, R)) = R.R^T \tag{2}$$

The size indicator of a zonotope is given by the Frobenius radius of $\mathbf{x}$ defined as [8] :

$$\|R\|_F = tr(R.R^T) \tag{3}$$

where $tr(.)$ is the trace of the matrix.

Let $b(R) \in \mathbb{R}^{n \times n}$ be a box that encloses the zonotope, $Z(c, R) \subset Z(c, b(R))$, with:

$$b(R) = diag(|R|\mathbf{1}) \tag{4}$$

$|.|$ represents the element-wise absolute value, $\mathbf{1}$ is a ones vector and $diag(.)$ allows the conversion from a vector to a diagonal matrix.

It is sometimes necessary to reduce the number of generator vectors in the generator matrix R to maintain a reasonable calculation time. The reduction operator, denoted $\downarrow q$, limits the number of generator vectors to q as described in [8]:

$$\begin{gathered} R = [r_1, ..., r_i, ..., r_m], \text{ such as } \|r_i\|_2 \geq \|r_{i+1}\|_2 \\ \text{if } m \leq q \text{ then } \downarrow_q R = R \\ \text{else } \downarrow_q R = [R_1, b(R_2)] \\ R_1 = [r_1, r_2, ..., r_{q-n}] \text{ and } R_2 = [r_{q-n+1}, r_{q-n+2}, ..., r_m]. \end{gathered} \tag{5}$$

It is interesting to note that sorting the vectors of the matrix R in descending order according to the L2-norm makes it possible to approximate, by a box, the vectors having the least influence on the zonotope size. Notice that the L2-norm can be replaced by the L1 and the infinity norms [12]. This latter is used in the rest of the paper.

Figure 1 summarizes the bounding box computation idea for a zonotope of three generator vectors in a two dimensional space: $R \in \mathbb{R}^{2 \times 3}$. The obtained bounding box (in blue) is the reduced zonotope with two generator vectors.

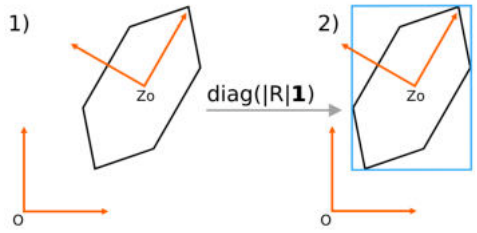

Fig. 1: The bounding box of the zonotope (in blue). Z_O the zonotope frame.

B. System modeling

Consider a system with stochastic and UBB uncertainties. The system can be described by the following evolution and observation models:

$$\mathbf{x}_{k+1} = f(\mathbf{x}_k, \mathbf{u}_k) + E_{z,k}.\mathbf{v}_{z,k} + E_{g,k}.\mathbf{v}_{g,k} \tag{6}$$

$$\mathbf{z}_k = h(\mathbf{x}_k) + F_{z,k}.\mathbf{w}_{z,k} + F_{g,k}.\mathbf{w}_{g,k} \tag{7}$$

With :

- $\mathbf{x}$ the state vector,
- $\mathbf{u}$ the input vector, for example, speed
- $\mathbf{z}$ the observation vector,
- $E_g\mathbf{v}_g \sim N(0, Q_{v_g})$ and $F_g\mathbf{w}_g \sim N(0, Q_{w_g})$ the process and observation noises modeled as white Gaussian noises with zero means and covariances $Q_{v_g} = E_g E_g^T$ and $Q_{w_g} = F_g F_g^T$ respectively,
- $E_z\mathbf{v}_z \sim Z(0, E_{v_z})$ and $F_z\mathbf{w}_z \sim Z(0, E_{w_z})$ the process and observation bounded noises modeled as zonotopes with zero means and covariations $Q_{v_z} = E_z E_z^T$ and $Q_{w_z} = F_z F_z^T$, respectively.

The choice of zonotope shape is justified by the computational and combination simplicity with the classical KF equations as it will be detailed in the next section.

C. Zonotopic and Gaussian Kalman Filter

The ZGKF was initially introduced in [8]. The derivation of the ZGKF is done based on Luenberger observer structure. Given a nonlinear model, the equations of the extended ZGKF will be directly given in this section.

The true state vector at instant k can be written as :

$$\mathbf{x}_k = \overline{\mathbf{x}}_k + \mathbf{g}_k + \mathbf{s}_k \tag{8}$$

With $\overline{\mathbf{x}}_k$ the estimated state vector at epoch k, $\mathbf{g}_k \sim N(0, P_k)$ the white Gaussian noise with zero mean and covariance P, $\mathbf{s}_k \sim Z(0, R_k)$ the zonotope bounded disturbance with zero mean and generator matrix R.

The ZGKF observer structure leads to the estimated state vector [8], [13], [14]:

$$\overline{\mathbf{x}}_{k+1} = (A_k - G_k H_k)\overline{\mathbf{x}}_k + B_k u_k + G_k z_k \tag{9}$$

with generator matrix

$$R_{k+1} = [(A_k - G_k H_k)\bar{R}_k, E_z, -G_k F_z] \tag{10}$$

and covariance matrix

$$P_{k+1} = (A_k - G_k H_k)P_k(A_k - G_k H_k)^T + Q_{v_{g,k}} + G_k Q_{w_{g,k}} G_k^T \tag{11}$$

$\bar{R}_k$ is the generator matrix after a reduction step. $A_k = \frac{\partial f}{\partial \mathbf{x}}|_{\mathbf{x}_k, u_k}$, $B_k = \frac{\partial f}{\partial u}|_{\mathbf{x}_k, u_k}$ and $H_k = \frac{\partial h}{\partial \mathbf{x}}|_{\mathbf{x}_k, u_k}$ are the Jacobian matrices used for linearization. G is the observer gain.

It can be observed from Equation 10 that the matrix R undergoes an update through concatenation, resulting in an increase in the number of generator vectors. The reduction step can be applied to limit the number of generator vectors.

Regarding the observer gain G, in the case of KF, it is obtained by minimizing the trace of the covariance matrix which is equivalent to minimizing the mean squared error. In the case of ZGKF, the optimal gain G is obtained by minimizing both zonotopic and Gaussian uncertainties. This can be done by minimizing a multi objective function as proposed in [8] :

$$J = (1 - \eta)tr(M_k) + \eta tr(P_k) \tag{12}$$

where $M = RR^T$ is the covariation matrix and $\eta \in [0, 1]$. η adjusts the weighting between the zonotopic and Gaussian components within the overall solution. The optimal gain is then:

$$G_k = A_k K_k \tag{13}$$

where

$$K_k = P_{MP,k} H_k^T S_k^{-1} \tag{14}$$

is analog to the classical Kalman gain and

$$S_k = H P_{MP,k} H_k^T + Q_{w,k} \tag{15}$$

is the analog to the innovation matrix. P_{MP} is the matrix that combines the covariance P (equation 11) and covariation $M = RR^T$ (equation 10) associated to the state vector:

$$P_{MP,k} = (1 - \eta)M_k + \eta P_k \tag{16}$$

$Q_{w,k}$ is the covariance and covariation matrix combination of the observation uncertainty such as $Q_{w,k} = (1 - \eta).Q_{w_z,k} + \eta.Q_{w_g,k}$.

The ZGKF can be now divided into the prediction and the update steps.

Prediction step: The predicted state vector $\mathbf{x}_{k+1|k} = f(\mathbf{x}_{k|k}, \mathbf{u}_k)$ has a generator matrix

$$R_{k+1|k} = [A_k R_{k|k}, E_{z,k}] \tag{17}$$

leading to a covariation matrix :

$$M_{k+1|k} = A_k M_{k|k} A_k^T + Q_{v_{z,k}}. \tag{18}$$

The predicted covariance matrix is computed in a similar way to the KF:

$$P_{k+1|k} = A_k P_{k|k} A_k^T + Q_{v_{g,k}} \tag{19}$$

As discussed before, the reduction is applied to $R_{k+1|k}$ to limit the size of the generator matrix :

$$\overline{R}_{k+1|k} = \downarrow_q R_{k+1|k} \tag{20}$$

and $\overline{M}_{k+1|k} = \overline{R}_{k+1|k}\overline{R}_{k+1|k}^T$.

The combination of the Gaussian covariance matrix with the covariation matrix leads to:

$$P_{MPk+1|k} = (1 - \eta)\overline{M}_{k+1|k} + \eta P_{k+1|k} \tag{21}$$

Update step: The updated state vector for the extended ZGKF is given by:

$$\mathbf{x}_{k|k} = \mathbf{x}_{k|k-1} + K_k.(z_k - h(\mathbf{x}_{k|k-1}, \mathbf{u}_k)) \tag{22}$$

where the zonotopic Gaussian Kalman gain is:

$$K_k = P_{MP,k|k-1} H_k^T S_k^{-1} \tag{23}$$

$$S_k = H_k P_{MP,k|k-1} H_k^T + Q_{w,k} \tag{24}$$

The updated generator matrix is:

$$R_{k|k} = [(I - K_k H_k)\overline{R}_{k|k-1}, -K_k F_{z,k}] \tag{25}$$

with associated covariation:

$$M_{k|k} = (I - K_k H_k)\overline{M}_{k|k-1}(I - K_k H_k)^T + K_k Q_{w_{z,k}} K_k^T \tag{26}$$

The covariance matrix associated to the Gaussian noise is:

$$P_{k|k} = (I - K_k H_k)P_{k|k-1}(I - K_k H_k)^T + K_k Q_{w_{g,k}} K_k^T \tag{27}$$

$P_{MP,k|k}$ can be obtained in a similar way to equation 16.

Regarding the multi-objective function, in our scenario and in absence of prior knowledge about the noises, there is no justification to favor either the Gaussian or UBB uncertainties. This corresponds to η being equal to 0.5. The multi-objective optimization with $\eta = 0.5$ is thereby simplified to mono-objective optimization, where the function J is:

$$J = tr(M) + tr(P) \tag{28}$$

This problem leads to the same prediction and update steps as for $\eta = 0.5$.

III. Robust Zonotopic and Gaussian Information Filter

A. Zonotopic and Gaussian Information Filter

In this section, we introduce and develop the informational form of the ZGKF, denoted as Zonotopic and Gaussian Information Filter (ZGIF). The ZGIF can be derived in a similar manner to the Information Filter (IF) [10]. The formulation is specifically well suited for multi-sensor data fusion and simplifies the management of sensor faults thanks to the summation of information contributions [15].

The ZGIF is mathematically equivalent to the ZGKF. However, it operates with an information matrix, Y_k, and information vector, $\mathbf{y}_k$, which are provided respectively as:

$$Y_k = {P_{MP}}_k^{-1} \tag{29}$$

$$\mathbf{y}_k = {P_{MP}}_k^{-1}\mathbf{x}_k \tag{30}$$

P_{MPk} is the combination of the covariance and covariation as in equation 16.

The prediction step of the ZGIF is similar to the ZGKF, with the addition of a step to transform from the state space to the informational space. For the update step, $P_{MPk|k}$ can be simplified to [8]:

$$P_{MPk|k} = (I - K_k H_k) P_{MPk|k-1} \tag{31}$$

Then,

$$(I - K_k H_k) = P_{MPk|k} {P_{MP}}_{k|k-1}^{-1} \tag{32}$$

Based on equation 23 and substituting $(I - K_k H_k)$ with equation 32, the zonotopic and Gaussian Kalman gain can be reorganized as follows:

$$K_k = P_{MPk|k} H_k^T Q_{w,k}^{-1} \tag{33}$$

Using these equations, the derivation of the ZGIF follows a similar approach to the IF [10]. The updated information matrix is then:

$$Y_{k|k} = Y_{k|k-1} + H_k^T Q_{w,k}^{-1} H_k \tag{34}$$

Notice that $Y_{k|k}$ includes the Gaussian (P) and zonotopic parts (M).

Using equations 32 and 33, the generator and covariation matrices (equations 25 and 26) can be written based on the informational form:

$$R_{k|k} = [Y_{k|k}^{-1} Y_{k|k-1} \overline{R}_{k|k-1}, \quad -Y_{k|k}^{-1} H_k^T Q_{w,k}^{-1} . F_{z,k}] \tag{35}$$

$$\begin{aligned} P_{k|k} = {} & Y_{k|k}^{-1} Y_{k|k-1} P_{k|k-1} Y_{k|k-1} Y_{k|k}^{-1} \\ & + Y_{k|k}^{-1} H_k^T Q_{w,k}^{-1} Q_{w_{g,k}} Q_{w,k}^{-1} H_k Y_{k|k}^{-1} \end{aligned} \tag{36}$$

As in the case of the IF, the information vector for linear system is obtained as

$$\mathbf{y}_{k|k} = \mathbf{y}_{k|k-1} + H_k^T Q_{w,k}^{-1} \mathbf{z}_k \tag{37}$$

Given the nonlinear system in section II-B, the information vector becomes

$$\mathbf{y}_{k|k} = \mathbf{y}_{k|k-1} + H_k^T Q_{w,k}^{-1} (\mathbf{z}_k - h(\mathbf{x}_{k|k-1}) + H \mathbf{x}_{k|k-1}). \tag{38}$$

In the case of multi-sensor data fusion with uncorrelated measurement noises, and following a similar approach to the IF, the information matrix and information vector can be modeled as:

$$Y_{k|k} = Y_{k|k-1} + \sum_{j=1}^{N} \mathbf{I}_{j_k} \tag{39}$$

$$\mathbf{y}_{k|k} = \mathbf{y}_{k|k-1} + \sum_{j=1}^{N} \mathbf{i}_{j_k} \tag{40}$$

where N is the number of measurements, $\mathbf{I}_{j,k}$ and $\mathbf{i}_{j,k}$ are the information contributions of observation $\mathbf{z}_{j,k}$:

$$\mathbf{I}_{j_k} = H_{j,k}^T Q_{w,j}^{-1} H_{j,k} \tag{41}$$

$$\mathbf{i}_{j_k} = H_{j,k}^T Q_{w,j}^{-1} (\mathbf{z}_{j,k} - h_j(\mathbf{x}_{k|k-1}) + H_{j,k} . \mathbf{x}_{k|k-1}) \tag{42}$$

Equations 39 and 40 distribute the computation of $\mathbf{I}_{j,k}$ and $\mathbf{i}_{j,k}$ efficiently thanks to the summation component. Equation 39 is then used for the computation of $R_{k|k}$ and $P_{k|k}$.

B. PCA based reduction step

The reduction step allows to limit the number of columns of the generator matrix which increases at each step due to the concatenation in equations 17 and 25. This reduction is essential for computational efficiency.

The reduction step can be seen as an over-approximation of the original zonotope by another zonotope Z_{red} of a smaller order. It is crucial that this over-approximation is as close-fitting as possible to ensure a high-quality state estimation and accurate representation of associated uncertainty values [16]. The classical reduction method presented in equation 5 involves a bounding box that is not oriented with the zonotope, as illustrated in figure 1. This reduction can lead to unnecessary large box. Furthermore, Z_{red} does not hold any information about the original zonotope orientation. To address this issue, in this paper, a principal components analysis (PCA) based oriented bounding box is applied as proposed in [12], to replace $b(R_2)$ in equation 5.

Consider a zonotope Z of dimension n and a generator matrix R of m generator vectors such as $m > n$. The PCA based over-approximation of Z, noted as $b_{pca}(R)$, consists in finding a matrix that transforms Z into a multidimensional oriented box [12]. This transformation matrix is obtained by finding the n most important directions by applying the singular value decomposition (SVD) on the matrix X obtained from the generator matrix R as follows:

$$L = [R, -R] \tag{43}$$

$$X = LL^T \tag{44}$$

The transformation matrix U is obtained as:

$$USV^T = svd(X) \tag{45}$$

$b_{pca}(R)$ is then

$$b_{pca}(R) = U.b(U^T.R) \tag{46}$$

where $b(.)$ is given in equation 4.

Figure 2 summarizes the PCA zonotope bounding box process. This PCA bounding box is used to perform the reduction during the ZGIF steps. Also, it will be used for bounding the errors as it will be detailed in section IV-B.

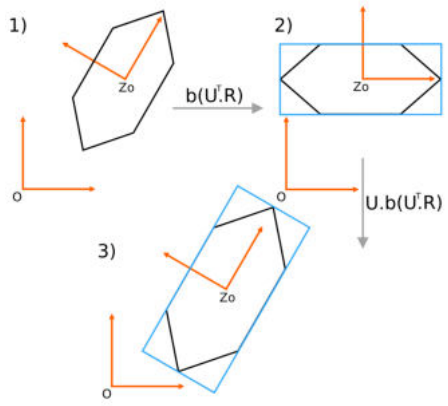

Fig. 2: The PCA zonotope reduction process steps. Step 1 to 2: the bounding box obtained from the most important directions. Step 2 to 3: the oriented bounding box of the zonotope.

C. Fault detection and exclusion

Even if the ZGIF can handle unknown but bounded errors, large errors can significantly impact the filter's state estimation. Therefore, we propose incorporating an FDE step to remove these errors from the fusion procedure.

The FDE architecture is based on a fault detection step using a global residual computed from the Mahalanobis distance between the predicted and the updated state vectors:

$$r_k = (\mathbf{x}_{k|k} - \mathbf{x}_{k|k-1}) Y_{k|k} (\mathbf{x}_{k|k} - \mathbf{x}_{k|k-1})^T \tag{47}$$

For the computation of r, all the measurements in the system are taken into account and $Y_{k|k}$ is given in equation 39. Since this residual incorporates both Gaussian and zonotope modeling, determining a theoretical threshold value based on a false alarm probability is not straightforward. Hence, for this work, the residual is compared to a threshold th_{glob} defined in an empirical way.

If a fault is detected using the global residual r, a bank of ZGIF is then employed to compute local residuals r_j, where each ZGIF in the bank uses only one observation $\mathbf{z}_{j,k}$:

$$r_{j,k} = (\mathbf{x}_{j,k|k} - \mathbf{x}_{k|k-1}) Y_{j,k|k} (\mathbf{x}_{j,k|k} - \mathbf{x}_{k|k-1})^T \tag{48}$$

$\mathbf{x}_{j,k|k}$ and $Y_{j,k|k}$ are obtained from the ZGIF filter which uses only the observation $\mathbf{z}_{j,k}$.

The residuals r_j are then compared to a local defined threshold. If r_j exceeds the threshold, the faulty measurement $\mathbf{z}_j$ is excluded by subtracting its information contribution from equations 39 and 40. The new value of $Y_{k|k}$ is used to update the covariance and generator matrices (equation 35 and 36). It is important to note that $R_{k|k}$ and $P_{k|k}$ are only computed when no more faults are detected in the system.

IV. Case Study

A. Localization of intelligent vehicles

Let's consider the localization of an intelligent vehicle equipped with wheel-speed sensors, a yaw-rate gyro, a GNSS receiver for pseudo-range measurements (with the antenna located at frame R_G, see figure 3), an intelligent camera for lane-marking detection, and an HD map. The localization task is defined relative to a local ENU frame (East, North, Up) denoted R_O. The vehicle's pose is defined in the body frame positioned at the midpoint of the rear wheel axis R_B (figure 3).

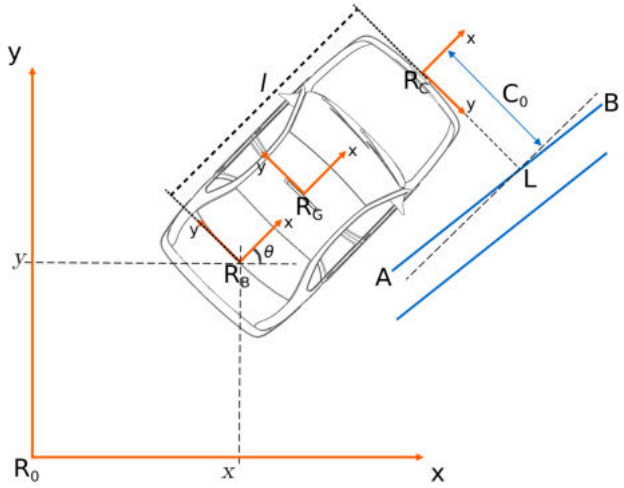

Fig. 3: R_B, R_G and R_C are the vehicle, GNSS and camera frames, respectively. The camera detects a lane marking $[AB]$.

The state vector at epoch k in a tightly coupled architecture is represented as:

$$\mathbf{x}_k = [x, y, z, \theta, cdt, \dot{cdt}]_k \tag{49}$$

In addition to the vehicle's position and heading, it includes the receiver clock offset cdt and clock drift $\dot{cdt}$ with respect to GPS time [17].

The GNSS observation model is given by :

$$\mathbf{z}_j = d_j + cdt + F_z.\mathbf{w}_z + F_g.\mathbf{w}_g \tag{50}$$

where d_j is the Euclidean distance between the GNSS receiver and the satellite j as given in [18]. In this work, we consider GPS and Galileo constellations. The noise associated with each observation is modeled using Gaussian and bounded noises, as detailed in section II-B. We leverage this modeling to enhance the integrity of the state estimation.

Another observation model based on the smart camera is used to improve localization in the cross-track direction by detecting lane markings. The camera can simultaneously detect up to four lane markings (two on each side) and provides a lateral distance (C_0). C_0 corresponds to the distance between the frame R_C and the intersecting point L on the map-matched segment $[AB]$ (figure 3).

The observation model associated to the camera is then :

$$\mathbf{z}_{cam} = C_0 + F_z.\mathbf{w}_z + F_g.\mathbf{w}_g \tag{51}$$

where the lateral distance C_0 is given as [19]:

$$C_0 = \frac{(l\sin\theta + y - y_A)x_{AB} - (l\cos\theta + x - x_A)y_{AB}}{x_{AB}\cos\theta + y_{AB}\sin\theta}. \tag{52}$$

l is the distance between R_B and R_C. More details can be found in [20]. The noises associated to the camera measurements are also modeled as Gaussian and bounded errors. In this case, the zonotope bounded noises are well-suited for addressing camera calibration issues.

For state estimation, the ZGIF with FDE proposed in section III is used. The prediction step uses the odometer data as input and models the noises as Gaussian and zonotopic bounded noises. The zonotopic noises are specifically adapted to account for gyro biases. The GNSS and camera measurements are used in the update step by computing their information contributions. Camera measurements are not always available, as the camera cannot detect markings on highly curved roads.

If a fault is detected using the global residuals (equation 47), a set of residuals r_j is computed as in equation 48 for each measurement (pseudo-range or camera). If r_j exceeds the threshold, the corresponding measurement is excluded by subtracting its information contribution from the main ZGIF filter, which uses all the observations.

B. Protection Level computation

In addition to achieving required accuracy, ensuring the integrity of localization of intelligent vehicles requires the computation of a consistent confidence interval. Originally developed for aeronautical applications, external localization integrity provides confidence in GNSS navigation solutions [9]. It includes a Target Integrity Risk (TIR), indicating the maximum probability of the Position Error (PE) exceeding a limit without alerting the user. This limit is known as the Protection Level (PL) :

$$p(PE > PL) \leq TIR. \tag{53}$$

In the context of intelligent vehicles, the PL must take into account all available sensors and potential errors that may arise in urban environments.

In this paper, the computation of PL considers the ZGIF modeling, incorporating both Gaussian and zonotopic components. The purpose is to take advantage of stochastic and set-membership modeling to compute a consistent PL that avoids underestimation resulting from undetected errors after the FDE step, non Gaussian distributions, or model linearization. The confidence box obtained from the ZGIF for a given confidence level α verifies:

$$p(er \in [-PL, PL]) \geq 1 - \alpha \tag{54}$$

$er = \mathbf{x}_k - \mathbf{x}_{k|k}$ is the difference between the true state and the estimated state (obtained from the ZGIF). As demonstrated in [8], the inequality relation results from the zonotope part $s \sim Z(0, R)$ that must verify $p(s \in Z(0, R)) = 1$. The Gaussian part bounds verifies the equality $1 - \alpha$. This equation can be written in an equivalent manner to equation 53:

$$p(|er| > PL) \leq \alpha \tag{55}$$

In [8], the authors determine the uncertainty region by using the bounding box presented in equation 4. However, the obtained bounding box is not aligned with the zonotope. In this paper, we propose to use the PCA bounding box, as defined in equation 46. Indeed, for intelligent vehicles, ensuring proper orientation of the bounding box is crucial when computing the PL. Specifically, for this case, it is essential to bound errors in both the along-track (AT) and cross-track (CT) directions. The protection level can be divided to:

$$PL_{xT} = PL_{xT,g} + PL_{xT,z} \tag{56}$$

The index xT refers to the AT or CT direction, $PL_{xT,g}$ is associated to the Gaussian part with $TIR = \alpha$ and $PL_{xT,z}$ is associated to the zonotope part.

The computation of PL_g in the AT and CT directions is done in a similar manner to [20], by projecting the eigenvectors of the covariance $P_{k|k}$ into the AT and CT directions (based on the orientation of the vehicle). The same idea is applied to the zonotope part (PL_z) where the eigenvectors $[U_1, \quad U_2]^T$ are directly obtained from the PCA step (equation 46). Therefore,

$$PL_{AT,z} = \max(\|r_1\|_2 \, |U_{1,AT}|, \|r_2\|_2 \, |U_{2,AT}|) \tag{57}$$

$$PL_{CT,z} = \max(\|r_1\|_2 \, |U_{1,CT}|, \|r_2\|_2 \, |U_{2,CT}|) \tag{58}$$

$[r_1, \quad r_2]$ is the generator matrix associated to the non oriented bounding box $b(U^T R)$ (figure 2 step 2) and $[U_{1,AT}, \quad U_{1,CT}]^T$, $[U_{2,AT}, \quad U_{2,CT}]^T$ are the eigenvectors in the (AT, CT) frame.

V. Experimental results

In this section, the proposed approach is evaluated using experimental data acquired from a Zoe vehicle navigating in a suburban environment over a trajectory of approximately 6 km, as illustrated in figure 4.

The vehicle was equipped with a Septentrio AsteRx SB PRO Connect for Galileo and GPS pseudorange measurements, wheel-speed sensors, a yaw-rate gyro, a Mobileye camera for lane marking detection, a SPAN CPT for ground truth, and an HD map. Acquisitions were conducted at 50Hz for dead reckoning, 3.5Hz for the camera, and 1Hz for GNSS measurements. The localization is delivered at 50Hz.

The performance of the ZGIF in terms of accuracy and integrity is evaluated both with and without the FDE procedure. Figure 5 illustrates the errors of the ZGIF in the AT and CT directions, before and after the FDE step. A notable improvement in localization accuracy can be seen after the FDE step, especially around $t = 0.5 \times 10^4$, where camera faults are detected. Figure 6 presents the residual used for fault detection, while figure 7 shows the residuals used to exclude camera faults. The faults mainly arise in camera

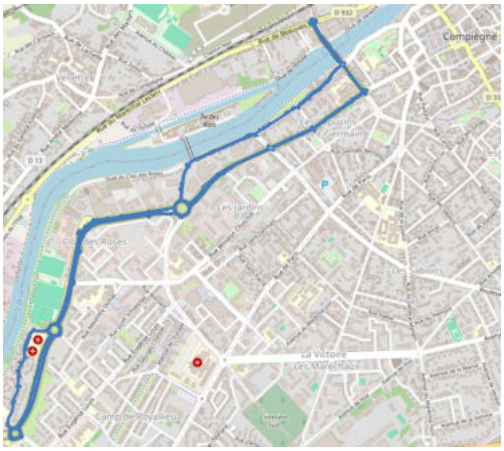

Fig. 4: Experimental trajectory (in blue) in Compiègne.

measurements, which may be prone to association issues with the HD map or may experience poor quality detection. For GNSS, fewer measurements are excluded. For example, a GPS pseudorange is excluded at the beginning of the trajectory due to low satellite elevation. Another GPS measurement is excluded around $t = 1.8 \times 10^4$ where the vehicle navigates around the university campus, encountering tall buildings that create a challenging GNSS environment.

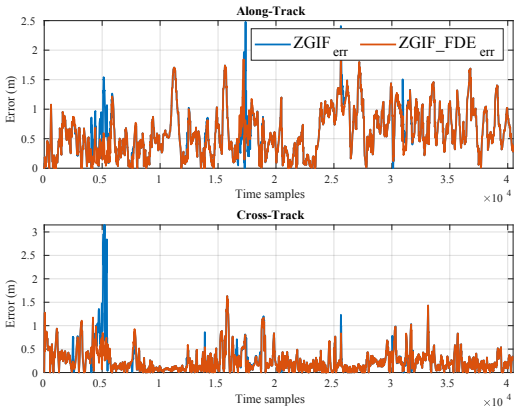

Fig. 5: Errors in the AT and CT directions before FDE (in blue) and after FDE (in red).

Table I presents the performance evaluation of the ZGIF regarding integrity and accuracy, including mean error and absolute error in both the AT and CT directions. It also provides a comparison to the classical IF (informational form of the KF).

The ZGIF and IF exhibit similar accuracy behaviors, with a slight improvement observed for the ZGIF. However, the ZGIF demonstrates superior integrity performance for a $TIR = 10^{-3}$. Without FDE, the ZGIF successfully verifies the integrity in the AT direction, with $IR = p(PE > PL) = 0 < 10^{-3}$, whereas the IF fails in this aspect. In the CT direction, while the ZGIF does not verify integrity, it demonstrates superior performance compared to the IF, that

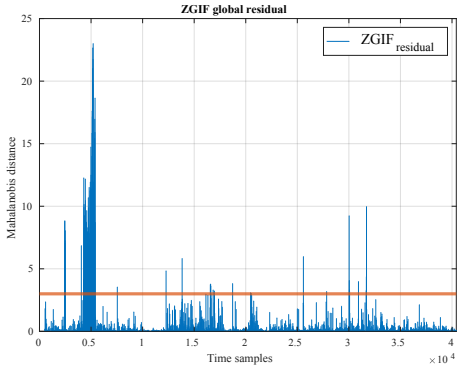

Fig. 6: Residual for fault detection (in blue) and associated threshold (in red).

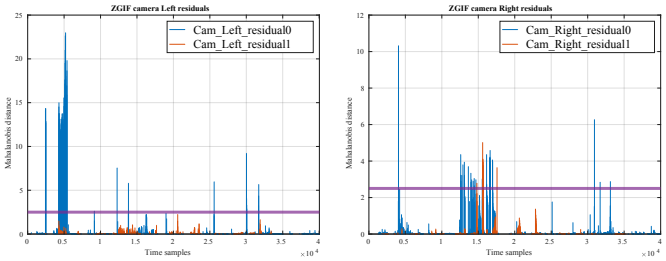

(a) Left side. (b) Right side.

Fig. 7: Camera residuals for fault exclusion (first measurement in blue, second in red). Threshold in purple.

shows high sensitivity to camera faults, resulting in an IR value significantly deviating from 10^{-3}. After the FDE step, the ZGIF meets the desired TIR in the AT and CT directions, while the IF does not. The interesting performance of the ZGIF originates from the modeling step that takes into account both Gaussian and bounded error.

Figure 8 shows the errors and PLs in the AT and CT directions. The PLs present mean values of 2.8m in the AT direction and 1.61 m in the CT direction. Compared to the IF, these values increased by 0.9m and 0.6m in the AT and CT directions, respectively. This increase is still acceptable. While the ZGIF enhances integrity, it manages to avoid the pessimism often associated with purely set-membership approaches. In

	ZGIF no FDE	ZGIF FDE	IF no FDE	IF FDE
|AT error| (m)	0.61	0.60	0.63	0.60
|CT error| (m)	0.27	0.24	0.27	0.24
|Mean error| (m)	**0.72**	**0.69**	0.74	0.70
IR_{AT} ($\times 10^{-3}$)	0	0	6.79	6.51
IR_{CT} ($\times 10^{-3}$)	7.85	0.54	37.9	15.1

TABLE I: Errors and Integrity Risk (IR) (per sample) for IF and ZGIF in the AT and CT directions ($TIR = 10^{-3}$). In green, integrity is verified.

the CT direction, the errors and PLs are influenced by the camera when detecting the markings, leading to a decrease in these values. It is worth noting that the camera does not influence the AT direction.

Regarding the choice of the zonotope reduction parameter, we opted for $q = 800$ to limit computational cost. However, selecting a smaller value of q would impact accuracy and lead to pessimistic PL values. For instance, without the FDE step, choosing $q = 25$ results in PLs with mean values of $4.57m$ in the AT direction and $2.91m$ in the CT direction. Furthermore, the ZGIF shows an increase in IR compared to $q = 800$, with values around 11×10^{-3} in both AT and CT directions. This result is mainly attributed to a decrease in accuracy, where the mean error increases from 0.74m with $q = 800$ to 0.96m with $q = 25$.

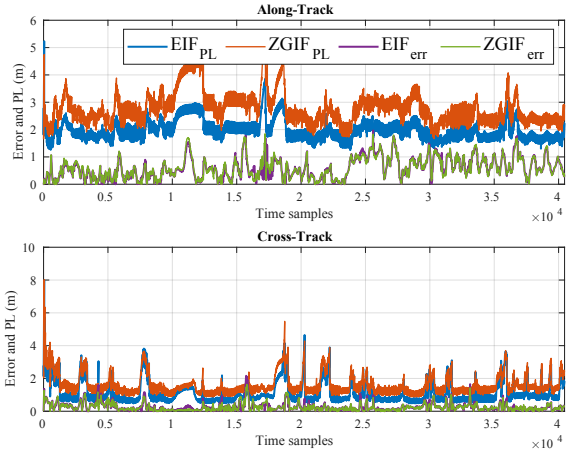

Fig. 8: Errors and PLs for ZGIF and EIF with FDE.

VI. Conclusion

In this paper, a novel robust ZGIF for multi-sensor data fusion and PL calculation was proposed. The filter exhibits the ability to handle random noise and set membership uncertainties. To enhance filter robustness and ensure high integrity localization, an FDE architecture is proposed. This step takes advantage of the ZGIF update step, which is modeled as a summation of information contributions. Experimental results conducted on an automated vehicle and using raw sensor data demonstrate the effectiveness of the proposed method in improving integrity compared to traditional KF without an overestimation of the uncertainty values.

The filter performance is highly dependent on filter parameters, e.g. noises covariance and covariation, detection threshold and reduction parameter. Future work will focus on parameter tuning based on data driven approach.

References

[1] W. Farag, "Self-driving vehicle localization using probabilistic maps and unscented-kalman filters," *International Journal of Intelligent Transportation Systems Research*, vol. 20, pp. 1–16, Jul. 2022.

[2] S. Katwe, N. Iyer, M. Khan, M. Peters, and M. Mahale, "Particle filter based localization of autonomous vehicle," in *2021 2nd Global Conference for Advancement in Technology (GCAT)*, 2021, pp. 1–6.

[3] S. Rohou, L. Jaulin, L. Mihaylova, F. Le Bars, and S. M. Veres, "Guaranteed computation of robot trajectories," *Robotics and Autonomous Systems*, vol. 93, pp. 76–84, 2017.

[4] A. Ehambram, L. Jaulin, and B. Wagner, "Hybrid interval-probabilistic localization in building maps," *IEEE Robotics and Automation Letters*, vol. 7, no. 3, pp. 7059–7066, 2022.

[5] B. Noack, F. Pfaff, and U. D. Hanebeck, "Combined stochastic and set-membership information filtering in multisensor systems," in *2012 15th International Conference on Information Fusion*, 2012, pp. 1218–1224.

[6] L. Sun, H. Alkhatib, J.-A. Paffenholz, and I. Neumann, "Georeferencing of a multi-sensor system based on set-membership kalman filter," in *2018 21st International Conference on Information Fusion (FUSION)*, 2018, pp. 1–5.

[7] T. A. Tran, C. Jauberthie, L. Trave-Massuyés, and Q. H. Lu, "An interval kalman filter enhanced by lowering the covariance matrix upper bound," vol. 31, no. 2, pp. 259–269, Jun. 2021.

[8] C. Combastel, "Merging kalman filtering and zonotopic state bounding for robust fault detection under noisy environment," *IFAC-PapersOnLine*, vol. 48, pp. 289–295, Dec. 2015.

[9] N. Zhu, J. Marais, D. Bétaille, and M. Berbineau, "Gnss position integrity in urban environments: A review of literature," *IEEE Transactions on Intelligent Transportation Systems*, vol. 19, no. 9, pp. 2762–2778, 2018.

[10] S. Grime and H. Durrant-Whyte, "Data fusion in decentralized sensor networks," *Control Engineering Practice*, vol. 2, no. 5, pp. 849–863, 1994.

[11] C. Combastel, "A state bounding observer based on zonotopes," in *2003 European Control Conference (ECC)*, 2003, pp. 2589–2594.

[12] A.-K. Kopetzki, B. Schürmann, and M. Althoff, "Methods for order reduction of zonotopes," in *2017 IEEE 56th Annual Conference on Decision and Control (CDC)*, 2017, pp. 5626–5633.

[13] Y. Wang and V. Puig, "Zonotopic extended kalman filter and fault detection of discrete-time nonlinear systems applied to a quadrotor helicopter," in *2016 3rd Conference on Control and Fault-Tolerant Systems (SysTol)*, 2016, pp. 367–372.

[14] A. Al-Mohamad, V. Puig, and G. Hoblos, "Zonotopic extended kalman filter for rul forecasting with unknown degradation behaviors," in *2020 28th Mediterranean Conference on Control and Automation (MED)*, 2020, pp. 574–579.

[15] J. Al Hage, M. E. El Najjar, and D. Pomorski, "Multi-sensor fusion approach with fault detection and exclusion based on the kullback–leibler divergence: Application on collaborative multi-robot system," *Information Fusion*, vol. 37, pp. 61–76, 2017.

[16] M. Althoff, "Reachability analysis and its application to the safety assessment of autonomous cars," Ph.D. dissertation, Technische Universität München, 2010.

[17] G. Falco, M. Pini, and G. Marucco, "Loose and tight gnss/ins integrations: Comparison of performance assessed in real urban scenarios," *Sensors*, vol. 2017, p. 27, Jan. 2017.

[18] J. Al Hage, N. Salvatico, and P. Bonnifait, "High integrity localization of intelligent vehicles with student's t filtering and fault exclusion," in *2023 IEEE 26th International Conference on Intelligent Transportation Systems (ITSC)*, IEEE, 2023, pp. 1341–1348.

[19] Z. Tao, P. Bonnifait, V. Fremont, J. GUSMAN, and S. Bonnet, "Road-centered map-aided localization for driverless cars using single-frequency gnss receivers," *Journal of Field Robotics*, vol. 34, May 2017.

[20] J. Al Hage, P. Xu, P. Bonnifait, and J. Ibanez-Guzman, "Localization integrity for intelligent vehicles through fault detection and position error characterization," *IEEE Transactions on Intelligent Transportation Systems*, vol. 23, no. 4, pp. 2978–2990, 2022.